



Velocity and Temperature Dissimilarity in the Surface Layer Uncovered by the Telegraph Approximation

Kelly Y. Huang¹ · Gabriel G. Katul² · Marcus Hultmark¹

Received: 21 December 2020 / Accepted: 22 May 2021 / Published online: 25 June 2021
© The Author(s), under exclusive licence to Springer Nature B.V. 2021

Abstract

The physicist and mathematician Shang-Keng Ma once commented that “the simplest possible variable is one that can have two values. If there is only one value, no variation is possible.” Guided by this dictum, the telegraphic approximation (TA) is applied to the streamwise velocity component and air temperature time series acquired in the first metre above the salt flats of Utah, USA. The TA technique removes amplitude variations and retains only zero-crossing behaviour in a turbulent series, thereby allowing for an isolated examination of the role of clustering in intermittency. By applying the TA technique, clustering properties are analyzed to uncover dissimilarity in temperature and velocity across unstable, near-neutral, and stable atmospheric stratification. The spectral exponents of the original and of the TA series are examined, with the inertial-subrange behaviour conforming to prior empirical relations and the energy-containing range exhibiting deviations. These two distinct scale regimes are observed in the standard deviations of the running density fluctuations of the TA series, delineating scaling behaviour between fine and large scales. In the fine scales, clustering is not appreciably affected by the stability regime and is higher than in the large scales. In the large scales, the temperature series exhibits stronger clustering with increasing stability, and higher clustering compared with the streamwise velocity component series under stable conditions. Amplitude variations are shown to mitigate intermittency in the small scales of velocity, but play only a minor role in intermittency for temperature. Last, the inter-pulse period probability distributions are explored and implications to self-organized criticality as models for TA turbulence are discussed.

Keywords Atmospheric surface layer · Clustering · Hot-wires · Intermittency · Inter-pulse distribution · Telegraph approximation

✉ Kelly Y. Huang
yichunh@princeton.edu

¹ Princeton University, Princeton, NJ, USA

² Duke University, Durham, NC, USA

1 Introduction

Dissimilarity between the turbulent streamwise velocity fluctuations u' and temperature fluctuations T' remains a recalcitrant problem in turbulence research (Sreenivasan and Antonia 1997; Shraiman and Siggia 2000; Lumley and Yaglom 2001). At large (or integral) scales, T' exhibits distinct ramp-cliff patterns that are not apparent in u' (Warhaft 2000). These patterns appear in boundary-layer studies even in the presence of thermal stratification, canopy turbulence, grid-generated turbulence, and several free shear turbulent flows (Gao et al. 1989; Warhaft 2000; Sreenivasan and Antonia 1997). Within the inertial subrange (a range of scales that are much smaller than the integral length scale but much larger than the Kolmogorov microscale), second-order moments of the temperature and velocity structure functions both exhibit approximate two-thirds scaling consistent with the Kolmogorov and the Kolmogorov–Obukhov–Corrsin hypotheses (Obukhov 1962; Antonia et al. 2009). However, higher-order structure functions suggest more intermittent patterns in T' than u' (Chambers and Antonia 1984; Warhaft 2000; Sreenivasan and Antonia 1997). This latter point is further underscored by a much larger time-derivative skewness magnitude in T' when compared with u' (Sreenivasan 1991). It has been suggested that the excess skewness in dT'/dt is due to the sharp fronts of ramp-cliff patterns (Celani et al. 2001; Katul et al. 2006; Zorzetto et al. 2018) thereby connecting intermittency within the inertial scales of T' with larger structures.

Two aspects characterize intermittency in turbulent flows—one related to properties of its positive versus negative excursions and another related to large amplitude variations within positive or negative states. To separate the two ingredients of intermittency, the so-called telegraphic approximation (TA) can be employed (Sreenivasan and Bershadskii 2006). The binary nature of the telegraphic approximation permits isolating event clustering in time without being influenced by amplitude variations. Hence, telegraphic approximation preserves the zero-crossing properties in the original time series but eliminates amplitude variations associated with the energetic state. Although intermittency at integral scales and within the inertial subrange for T' and u' in the atmospheric surface layer (ASL) has been studied previously (Chambers and Antonia 1984; Shi et al. 2005), the clustering behaviour isolated from amplitude variations has rarely been considered except in a handful of studies (Cava and Katul 2009; Cava et al. 2012, 2019; Chowdhuri et al. 2020; Li and Fu 2013; Liu and Hu 2020; Poggi and Katul 2009). Moreover, memory in switching properties (positive-to-negative or negative-to-positive excursions) and persistence in one of the two states across turbulent scales is beginning to receive closer attention (Cava et al. 2012; Chamecki 2013; Chowdhuri et al. 2020). The switching properties have been linked to systems exhibiting self-organized criticality (SOC), a topic that has received attention and controversy starting from the original work of Per Bak (Bak et al. 1988; Sreenivasan et al. 2004). These issues motivate the present study.

This work inquires about the role of thermal stratification on clustering, persistence and intermittency of u' and T' in the ASL close to the ground. To what extent does the TA technique uncover dissimilarity between u' and T' across various thermal stratification levels? Does the excess intermittency in T' at inertial scales originate from clustering differences or amplitude variability when compared to u' ? Are the distributional properties of the negative events in u' and T' dissimilar across different thermal stratification? To what extent do analogies to SOC apply to T' and u' ? Answering these questions is the main compass of the experiments and analysis here. The experiments reported here offer a unique perspective as well because of their high sampling frequency (>100 Hz) and proximity to the ground (0.06–1.0 m).

Throughout, the following notation is used: x , y , and z indicate longitudinal (along mean wind direction), lateral, and vertical directions, respectively. The variables U , V , W are the instantaneous velocity components along the x , y , and z directions, respectively, with $U = \bar{U} + u'$, $V = \bar{V} + v'$, and $W = \bar{W} + w'$, where the overline indicates time averaging over a 30-min interval and primed quantities indicate deviations from time-averaged quantities. The coordinate system is selected so that $\bar{V} = \bar{W} = 0$. The instantaneous air temperature $T = \bar{T} + T'$ is also needed to assess the role of buoyancy generation or destruction of turbulent kinetic energy. In the ASL, atmospheric stability is quantified in one of two ways (Garratt 1994; Wyngaard 2004). The Monin–Obukhov stability parameter $\zeta = z/L$, where L is the Obukhov length given by

$$L = -\frac{u_*^3}{\kappa (g/\bar{T}) \overline{w'T'}}, \quad (1)$$

and the flux Richardson number R_f defined as

$$R_f = \frac{(g/\bar{T}) \overline{w'T'}}{\overline{w'u'}(d\bar{U}/dz)}, \quad (2)$$

where $u_* = \sqrt{-\overline{w'u'}}$ is the friction velocity, g is the acceleration due to gravity, and κ is the von Kármán constant. The two atmospheric stability representations are related by $R_f = \zeta/\phi_m(\zeta)$, where $\phi_m(\zeta)$ is the stability correction function for momentum discussed elsewhere (Katul et al. 2011; Salesky et al. 2013).

2 Experimental Set-Up

The data were collected at the Surface Layer Turbulence and Environmental Science Test (SLTEST) facility, located in the western deserts of Utah, USA. A 3-day intensive sampling period (20 to 22 June 2018) was conducted as part of the Idealized horizontal Planar Array study for Quantifying Surface heterogeneity (IPAQS) (Morrison et al. 2021). The site is known for its near-canonical nature due to a low surface roughness and long uninterrupted stretches of land in the dominant wind directions. Detailed description of the site can be found elsewhere (Klewicki et al. 1998; Metzger and Klewicki 2001).

Longitudinal velocity component U and air temperature T measurements were simultaneously sampled in the ASL at 100 Hz in the first metre above ground using nanoscale hot- and cold-wires operated in constant-current anemometry mode. The sensing element of the nanoscale thermal anemometry probe (NSTAP) is a platinum wire filament 100 nm in thickness, 2 μm in width and 60 μm in length, while the sensing element of its variant for temperature measurements (T-NSTAP) is also a platinum wire of the same thickness and width but slightly longer at 200 μm (Vallikivi and Smits 2014; Fan et al. 2015; Arwatz et al. 2015). Unlike conventional instrumentation used in atmospheric turbulence studies (i.e. sonic anemometers), the small size of the nanoscale sensors provides unprecedented spatial resolution that is able to resolve the smallest length scales in the flow and ensure minimal spatial filtering. By contrast, insufficient resolution of the spatial structure results in spatial aliasing in the direction aligned with the sensor, and ultimately leads to artificially low measurements, an effect that can be seen in any instrumentation that integrates thermodynamic effects over space (Citriniti and George 1997). Although they could certainly be sampled at

Table 1 Mean flow properties and stability classifications relative to the sonic anemometer positioned at $z = 2$ m for the 30-min periods analyzed (local time = UTC + 6 h)

Date	Local time	\bar{U} (m s ⁻¹)	ζ	R_f	Stability
20/06/2018	2230	2.47	0.27	0.083	Stable
21/06/2018	2000	7.55	0.025	0.014	Near-neutral
	2030	6.56	0.053	0.040	Near-neutral
	2100	6.02	0.057	0.034	Near-neutral
	2200	6.60	0.056	0.035	Near-neutral
	2230	7.34	0.038	0.034	Near-neutral
22/06/2018	0430	4.00	0.19	0.091	Stable
	0500	3.14	0.12	0.077	Stable
	0800	4.10	-0.13	-0.18	Unstable
	0830	3.86	-0.13	-0.23	Unstable

The parameters \bar{U} and ζ were calculated using the sonic anemometer data, while R_f was estimated from both the sonic anemometer data and the mean velocity profile given by the NSTAPs and evaluated at $z = 2$ m

higher frequencies, the sensors were sampled at 100 Hz for this initial deployment and do not capture the dissipation range behaviour.

Five stations of simultaneously sampling NSTAPs and T-NSTAPs were spaced on an approximately logarithmic scale at heights $z = 0.0625, 0.125, 0.25, 0.5,$ and 1.0 m above the ground. Due to sensor breakage, not all sampling heights are represented in the analysis below. Trends caused by a varying freestream velocity were removed following the methodology of Hutchins et al. (2012) and frequency components lower than 300^{-1} Hz were filtered out. Out of 92 30-min records collected, 77 records were discarded due to misalignment between the incoming flow and the sensors, and five were discarded due to non-stationary effects. The resulting 10 records are summarized in Table 1 and classified as unstable when $\zeta < -0.1$, near-neutral when $|\zeta| \leq 0.1$, and stable when $\zeta > 0.1$. The stationarity of the mean longitudinal velocity component \bar{U} and the turbulence intensity σ_u/\bar{U} at each measurement height was verified using the reverse arrangement test and the runs test with a 95% confidence interval (Bendat and Piersol 2011).

For a smooth wall, the onset of the logarithmic layer taken to be $z^+ = zu_*/\nu > 100$ (Valikivi et al. 2015) places the lowest sampling height of $z^+ \approx 850$ well within the logarithmic region. Under near-neutral conditions, the equivalent sand grain roughness was estimated to be ≈ 2.5 mm with the relation for a zero-pressure-gradient neutral boundary layer as discussed in Huang et al. (2021), so that the lowest sampling height is about 25 times that of the roughness height. However, recent evidence suggests that the extent of the buffer layer may be a function of the Reynolds number $\delta^+ = \delta u_*/\nu$ and extend to $z^+ \approx 3(\delta^+)^{1/2}$ in smooth-wall conditions (Marusic et al. 2013; Wei et al. 2005). Using this criterion and the boundary-layer thickness estimated under near-neutral conditions (as discussed in Huang et al. 2021), this results in an onset of the logarithmic layer at $z^+ \approx 2700$ so that the lowest two measurement heights would be within the buffer region below, where sweeps tend to dominate and contribute to the positive skewness values observed in Fig. 2 (Heisel et al. 2020). More details regarding the experimental set-up can be found in Huang et al. (2021).

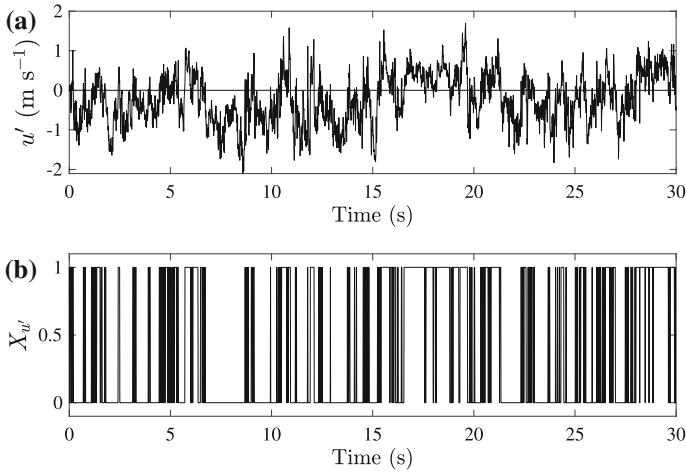


Fig. 1 Example of a $u'(t)$ series (a) and its corresponding TA series $X_{u'}$ (b) collected at $z = 0.25$ m with $\overline{U} = 5.3$ m s⁻¹

3 Method of Analysis

The telegraphic approximation of a turbulent series isolates clustering effects from amplitude variations by prescribing a magnitude of one when the turbulent series exceeds the mean value (or another threshold) and a magnitude of zero when it does not. By construction, a TA series is a binary series with no information on amplitude variations and retains only clustering (or zero-crossing statistics) information from the original series. Mathematically, the TA series of a fluctuating flow variable $s'(t)$ at time t is calculated as

$$X_{s'} = \frac{1}{2} \left(\frac{s'(t)}{|s'(t)|} + 1 \right), \tag{3}$$

where the straight brackets denote a time average. To illustrate, Fig. 1 shows a 30-s period of $u'(t)$ and its TA series measured at $z = 0.25$ m.

The following discussion assumes Taylor’s frozen turbulence hypothesis to convert temporal to one-dimensional spatial cuts along x . To minimize distortions arising from the usage of Taylor’s hypothesis, time scales are normalized by the integral time scale Λ_t of a flow variable s' that is given by

$$\Lambda_t = \int_0^\infty \rho_s(\tau) d\tau, \tag{4}$$

where $\rho_s(\tau) = \overline{s'(t)s'(t + \tau)}/s'^2$ is the temporal autocorrelation function of s' at time lag τ . The integration in Eq. 4 is, in practice, terminated at the first zero-crossing of the autocorrelation function. This normalized scale variable can be interpreted in space as relative eddy sizes when Taylor’s frozen turbulence hypothesis is invoked. Because distortions introduced by Taylor’s hypothesis affect simultaneously the numerator and denominator, the scale ratio $\tau \overline{U}/(\Lambda_t \overline{U})$ is more robust to such distortions.

3.1 Non-Gaussianity and the Telegraph Approximation

As discussed elsewhere (Poggi and Katul 2009), the TA technique preserves the non-Gaussian properties of any flow variable s' via Γ_+ , the fraction of time $s' > 0$. For illustration, the case where the probability density function (p.d.f.) of s' can be approximated using a third-order cumulant expansion is considered. That is,

$$p(s'_n) = G(s'_n) \left[1 + \frac{1}{6} Sk_s (s_n'^3 - 3s'_n) \right], \tag{5}$$

where $s'_n = s'/\sigma_s$ is normalized to zero-mean and unit variance, $\sigma_s = \sqrt{s'^2}$ is the standard deviation of s' , $Sk_s = \overline{s_n'^3}$ is the skewness of s' , and $G(s'_n) = (2\pi)^{-1/2} \exp(-s_n'^2/2)$ is the Gaussian p.d.f. In this case, the fraction of time the process exhibits positive excursions (i.e. $X_{s'} = 1$) is given by

$$\Gamma_+ = \int_0^\infty p(\xi) d\xi = \frac{1}{2} - \frac{1}{12} \sqrt{\frac{2}{\pi}} Sk_s. \tag{6}$$

Inclusion of the kurtosis (often linked to intermittency as discussed elsewhere (Townsend 1976)) via a fourth-order cumulant expansion of $p(s'_n)$ (instead of third-order) does not alter the above linear relation between Γ_+ and Sk_s . A similar expression can be derived for the negative excursions (Γ_-) given by

$$\Gamma_- = \int_{-\infty}^0 p(\xi) d\xi = \frac{1}{2} + \frac{1}{12} \sqrt{\frac{2}{\pi}} Sk_s. \tag{7}$$

Thus, the imbalance $\Delta\Gamma$ is given by

$$\Delta\Gamma = \Gamma_+ - \Gamma_- = -\frac{1}{6} \sqrt{\frac{2}{\pi}} Sk_s. \tag{8}$$

For a Gaussian distributed s' , $\Delta\Gamma = 0$. The expression in Eq. 8 is to be explored across different ζ regimes and for u' and T' .

3.2 Spectral Exponents

While the prior section illustrates how skewness is globally captured by the TA technique, this section describes how correlations (or spectral density functions) are encoded. It was demonstrated empirically from several numerically generated stochastic series that when the power spectral density of the original series scales as f^{-n} and that of its TA series as f^{-m} ,

$$m = \frac{n + 1}{2}, \tag{9}$$

where f is the frequency, n is the spectral exponent of the original series and m of its TA series (Sreenivasan and Bershadskii 2006). This result holds for both velocity and passive scalars.

In the inertial subrange where $n = 5/3$, Eq. 9 predicts $m = 4/3$ in the TA series, or a slower spectral decay rate. Generally, $m < n$ indicates that there is more ‘memory’ in the TA series than in the original time series; that is, amplitude variations seem to have ‘de-correlating’ effects on the series. The applicability of Eq. 9 to scales associated with larger eddies (e.g. attached to the wall) as well as any thermal distortions to them are considered here. For

scales larger than the inertial scales for both u' and T' under near-neutral conditions, $n = 1$ (which corresponds explicitly to wall-attached eddies and are discussed in Townsend (1976); Perry et al. (1986); Banerjee and Katul (2013); Katul et al. (2012); Li et al. (2016)) yields a predicted $m = 1$ for the TA series, the same spectral decay rate as its original signal. For non-neutral conditions, the value of the spectral exponent n is dependent on the stability regime and can be found elsewhere (see e.g. Chamecki et al. 2017).

3.3 Clustering Exponents

The clustering tendency of a signal is characterized by the clustering exponent α . The average density n_τ of zero-crossings is first determined by counting the number of zero-crossings within a time interval τ and then normalizing by the number of points in that time interval (note that this is the same zero-crossing information as in the original signal). The clustering exponent α is then determined from the scaling behaviour of the standard deviation of the running density fluctuations $(\delta n_\tau^2)^{1/2}$ with τ , where $\delta n_\tau = n_\tau - \langle n_\tau \rangle$, and the angled brackets denote time averaging for window size τ . That is,

$$(\delta n_\tau^2)^{1/2} \sim \tau^{-\alpha}. \tag{10}$$

For reference, it can be determined analytically that white noise, which exhibits no clustering behaviour, has a clustering exponent of $\alpha = 0.5$. Sreenivasan and Bershadskii (2006) empirically showed that as the Taylor microscale Reynolds number $Re_\lambda \rightarrow \infty$, $\alpha \rightarrow 0.1$ such that finite clustering persists. They also observed that for $200 < Re_\lambda < 20,000$, the clustering exponent α ranged from 0.25 to 0.4 for scales in the dissipative and inertial ranges, but is approximately a white noise value of $\alpha = 0.5$ for scales larger than the integral scale of the flow.

3.4 Intermittency Exponents

The variance dissipation rate of s' is characterized by the quantity

$$\xi(t) = \left| \frac{ds(t)}{dt} \right|^2. \tag{11}$$

Its local average, as first introduced by Obukhov (1962),

$$\xi_\tau = \frac{1}{\tau} \int_t^{t+\tau} \xi(t) dt, \tag{12}$$

is used to determine the intermittency exponent μ_q from scaling of its q^{th} moment,

$$\frac{\langle \xi_\tau^q \rangle}{\langle \xi_\tau \rangle^q} \sim \tau^{-\mu_q}. \tag{13}$$

A non-zero μ_q value indicates that there is a clusterization of pulses and the series is intermittent. By contrast, a uniform random distribution of pulses with no clusterization yields $\mu_q = 0$. To compare with previous literature, only μ_2 ($q = 2$) is considered. Going forward, μ_s denotes μ_2 of the original series, and μ_{TA} of the corresponding TA series.

Determined from the original series, μ_s contains information on both clusterization and amplitude variations, while μ_{TA} retains only information on clusterization. As noted earlier, intermittency is composed of two aspects, one related to amplitude variability and one related

to clustering. It follows that a comparison of the magnitudes of μ_{TA} and μ_s could indicate the role of amplitude variability in the observed intermittency. That is, $\mu_{TA}/\mu_s > 1$ suggests that amplitude variations mitigate intermittency; $\mu_{TA}/\mu_s < 1$ that amplitude variations amplify intermittency; and $\mu_{TA}/\mu_s \sim 1$ that much of the observed intermittency is due to clusterization and not amplitude variability.

3.5 Probability Density Function of the Inter-pulse Period

Lastly, the p.d.f. of the inter-pulse period is considered. The inter-pulse period I_p is defined as the interval of time between successive zero-crossings, or

$$I_p(i) = \widehat{t}_{i+1} - \widehat{t}_i, \quad (14)$$

where \widehat{t}_i is the time of the i th zero-crossing. The p.d.f. of I_p , $p(I_p)$, can be related to persistence defined as the probability that the local value of a fluctuating quantity s' does not change sign up to a time I_p (Sreenivasan et al. 1983; Kailasnath and Sreenivasan 1993; Chamecki 2013). As a result, $p(I_p)$ is also referred to as the persistence p.d.f.

The statistical characteristic describing the persistence p.d.f. continues to draw significant attention (Chowdhuri et al. 2020). Sreenivasan and Bershadskii (2006) showed that the probability law of the persistence p.d.f. may offer a classification of turbulence. A log-normal distribution, which is characteristic of a white noise process, classifies turbulence as ‘passive’ (i.e. for a passive scalar in shear-driven turbulence). On the other hand, a power-law scaling such that

$$p(I_p) \sim I_p^{-\gamma} \quad (15)$$

classifies turbulence as ‘active’ (i.e. in convective turbulence). More recently, studies have shown support for the persistence p.d.f. to follow a power-law distribution with an exponential cut-off (a stretched exponential) (Chowdhuri et al. 2020; Cava et al. 2012; Chamecki 2013). The occurrence of power laws (or stretched exponentials) in the persistence p.d.f. is of interest to phenomenological models of turbulence. Jensen et al. (1989) formally showed that for systems near critical behaviour,

$$m = 3 - \gamma. \quad (16)$$

Further, to account for intermittency Bershadskii et al. (2004) modified the relation to

$$m = 3 - \gamma - \mu/2. \quad (17)$$

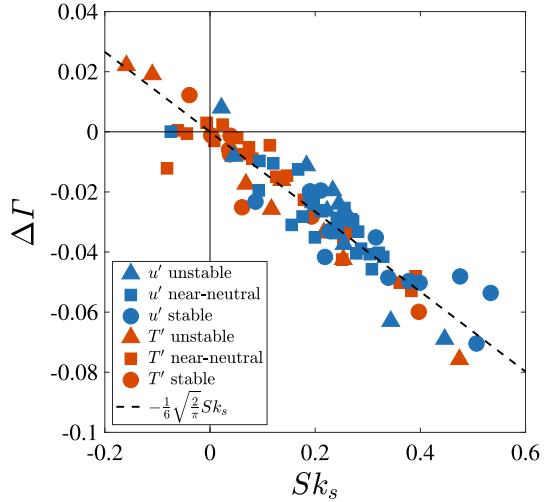
Hence, μ inferred from m and γ for u' and T' across different stability regimes may also offer new perspectives about intermittency and clustering in the ASL.

4 Results and Discussion

4.1 Non-Gaussianity and the Telegraph Approximation

To explore whether the TA technique preserves the non-Gaussian properties of the original time signal, $\Delta\Gamma$ as defined in Sec. 3.1 is presented against the skewness Sk_s of the original series for both u' and T' for each dataset summarized in Table 1 for all heights in Fig. 2. For all cases, the agreement of the results with Eq. 8 indicates that the TA series is able to capture the skewness of the p.d.f. of the original times series.

Fig. 2 Scatter plot of $\Delta\Gamma$, the difference between the fraction of time the turbulent fluctuations are positive and negative, against the corresponding skewness Sk_s of the original signal for both u' and T' for each dataset listed in Table 1 and for all available heights



The ability of the TA technique to preserve skewness via the fraction of time the signal exhibits positive versus negative excursions has also been shown in TA studies of other flows (Cava et al. 2012), and demonstrates that non-Gaussianity in the flow is related to not only amplitude variations (as demonstrated by Katul 1994; Giostra et al. 2002), but also to clusterization, the other aspect of intermittency.

4.2 Spectral Exponents

The u' and T' spectra were computed using standard fast Fourier transforms with constant levels of electronic noise subtracted. The spectra of the original series and of its TA series under near-neutral conditions for both u' and T' are shown in Fig. 3 as an example. For reference, f^{-1} and $f^{-5/3}$ are presented for the original series (Fig. 3a, c), and the corresponding f^{-1} and $f^{-4/3}$ scalings predicted by Eq. 9 for the TA series (Fig. 3b, d).

For each spectrum, two spectral exponents were determined: one from the large scales (that includes attached eddies), and one from finer scales in the inertial subrange. The energy-containing range was defined as $(6\Lambda_t)^{-1} < f < (\Lambda_t/6)^{-1}$ in accordance with Pope (2000), where Λ_t is defined as in Eq. 4 and averaged across the available runs for each stability regime and each height. The inertial subrange was defined to start at $f = (\Lambda_t/6)^{-1}$ and ends just before noise sets in for each run. As a result, each variable and height have different frequency values that define the two scaling regimes, as indicated by the groups of vertical lines in Fig. 3.

To explore the relation between the spectral exponents m and n , and the validity of Eq. 9 to scales associated with larger, attached eddies, exponents from both the energy-containing and inertial regions are represented in Fig. 4, and exponents from the respective regions in Fig. 5. Further, a synthetic turbulence series was generated from each spectrum by randomizing its phase angle while preserving its shape to examine whether the relation between m and n is an exclusive property of turbulence related to the Navier–Stokes equations. The spectral exponents of the phase-randomized series are also calculated and represented by open markers in each figure.

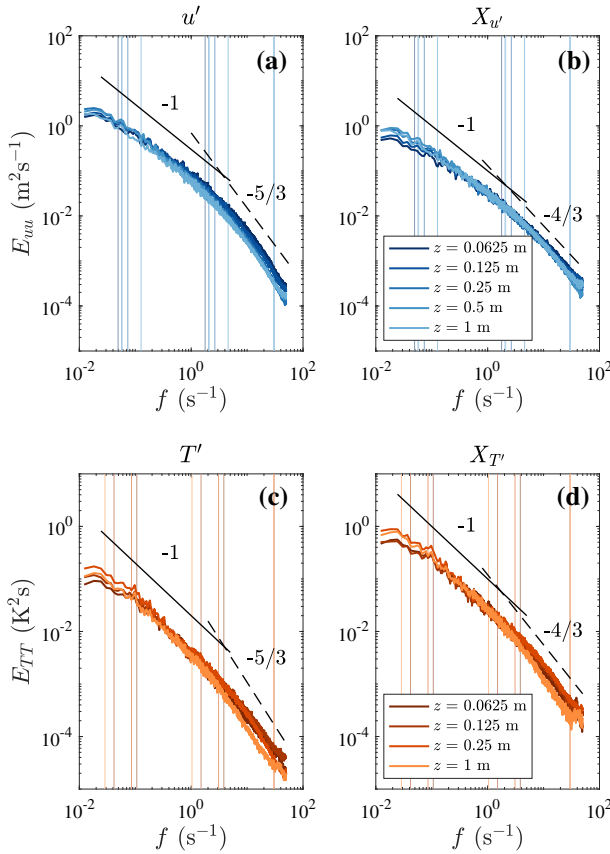


Fig. 3 Ensemble-averaged energy spectra of the original u' signal (a) and its TA series (b) and of the original T' signal (c) and its TA series (d) as a function of frequency f for near-neutral conditions. The vertical lines represent the frequencies used to calculate m and n ; from left to right, the groups of vertical lines correspond to $(6\Lambda_T)^{-1}$, $(\Lambda_T/6)^{-1}$, and the frequency before noise sets in

When data from both regions and for both u' and T' are considered (Fig. 4), despite deviations from the $n = 1$ scaling in the energy-containing range and the $n = 5/3$ in the inertial subrange, the linearity $m = an + b$ holds (where in Eq. 9, $a = b = 1/2$), confirming that the TA spectra contain significant information about the scaling laws of the original spectra for both velocity and scalar time series. This was also demonstrated by a number of other studies that examined this relationship in the inertial subrange (Sreenivasan and Bershadskii 2006; Cava and Katul 2009; Cava et al. 2012), among which the exact values of a and b differ. The current data exhibit a linear regression with $a = 0.60$ and $b = 0.33$, as compared to $a = b = 1/2$ found by Sreenivasan and Bershadskii (2006). A regression fit that deviated from that of Sreenivasan and Bershadskii (2006) was also observed by Cava and Katul (2009) in the canopy sublayer when combining all flow variables including scalars ($a = 0.66$ and $b = 0.09$), which is also plotted in Fig. 4 for reference.

To delineate the large- and small-scale behaviours, the results are considered by their respective regions. For energy-containing eddies, the relation between m and n exhibits a higher slope and lower intercept at $a = 0.75$ and $b = 0.16$. That is, for scales associated with

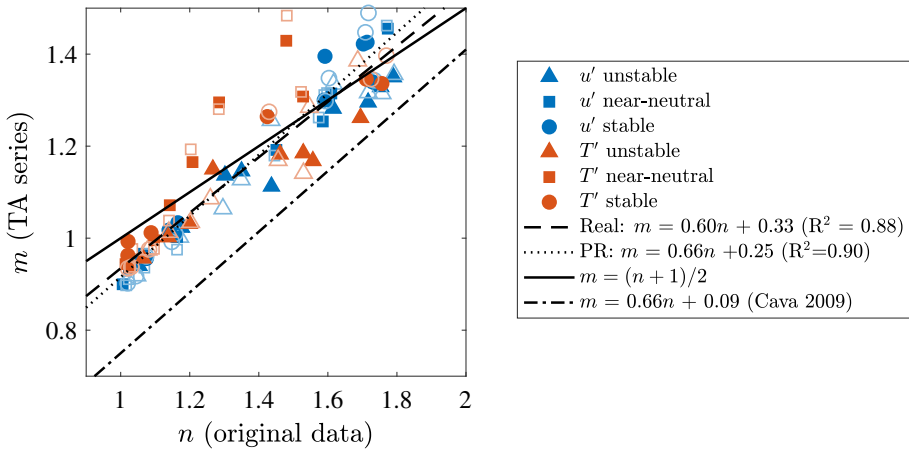


Fig. 4 Scatter plot of the spectral exponents of the original data (n) and of the corresponding telegraph approximations (m) calculated from ensemble-averaged energy spectra for each stability regime for both u' and T' and for each available height. The filled markers represent the real data, while the open markers represent the corresponding phase-randomized, synthetic data (denoted “PR” in the legend)

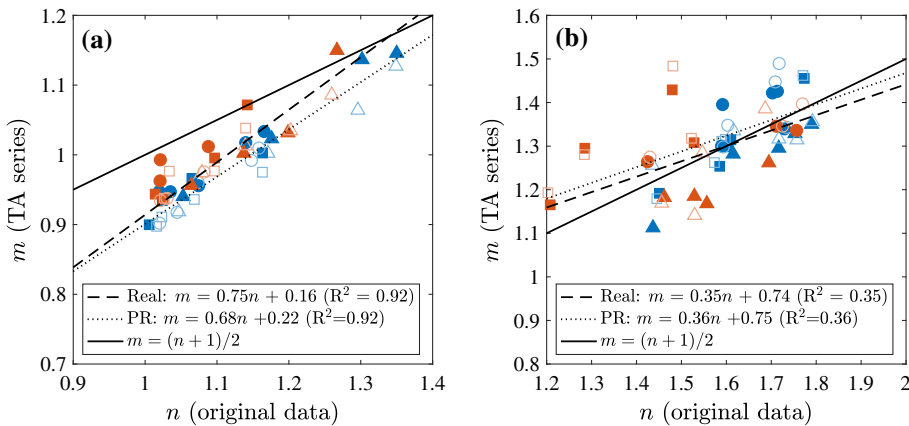


Fig. 5 As Fig. 4 but for the energy-containing region only (a) and for the inertial subrange only (b)

attached eddies, the $m = (n + 1)/2$ expression derived for turbulence far from boundaries generally overestimates the observed spectral slope of the TA series. This suggests that while linearity between m and n holds, a different scaling relation exists for the energy-containing range. However, the limited number of datasets prevents any significant insight being drawn on the exact values of a and b for this region. On the other hand, the relation for data in the inertial subrange, presented in Fig. 5b, does not appear to be statistically different than the relation proposed by Sreenivasan and Bershanskii (2006) given the scatter in the data.

The synthetic, phase-randomized data are not statistically different than the real turbulence data. This finding suggests that the relation between the original spectral exponent n and the TA spectral exponent m is not an exclusive property related to the temporal evolution of turbulence through the Navier–Stokes equations, but rather a property of stochastic processes.

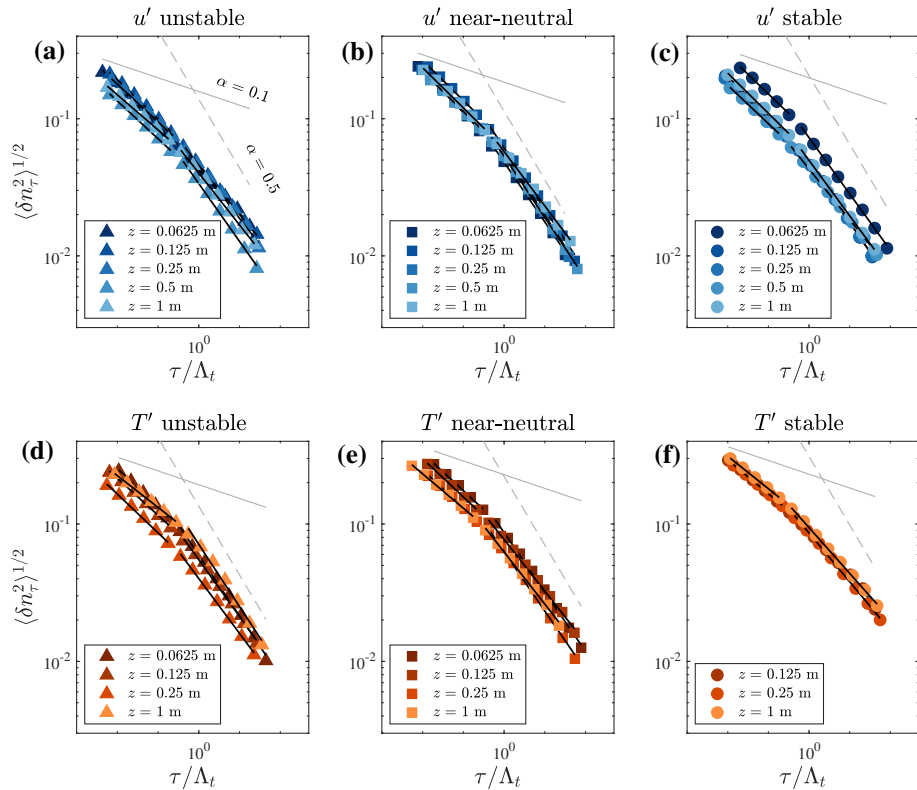


Fig. 6 Standard deviations for the running zero-crossing density fluctuations for u' under unstable (a), near-neutral (b), and strongly stable (c) stability regimes, and for T' under unstable (d), near-neutral (e), and strongly stable (f) stability regimes. For each variable and each height, the standard deviations are ensemble-averaged across cases with the same stability regime as given in Table 1. As a reference, the values for white noise ($\alpha = 0.5$) and for the limit $Re \rightarrow \infty$ ($\alpha = 0.1$) are also featured. The straight black lines are best-fits that indicate the scaling laws of the two regions separated at $\tau/\Lambda_t \sim 1/6$

Whether the observed slope of the linear relation is a stochastic property specific to wall-bounded turbulent flows remains to be explored.

4.3 Clustering Exponents

Figure 6 presents the standard deviations of the zero-crossing density fluctuations $(\delta n_\tau^2)^{1/2}$ as a function of τ/Λ_t , where Λ_t is the integral time scale. There is a visible break in scaling behaviour at $\tau/\Lambda_t \sim 1$, indicating a difference in clustering tendencies between the fine scales (those in the inertial subrange) and the large scales (those associated with energy-containing eddies). For the current analysis, the demarcation between the two ranges of scales was taken to be $\tau/\Lambda_t = 1/6$ in accordance with the cut-off frequency in calculating the spectral exponents. As reference, $\alpha = 0.1$ in the limit of infinite Re_λ as predicted by Sreenivasan and Bershadskii (2006) and $\alpha = 0.5$ representative of a white noise process (with no clustering behaviour) are also plotted.

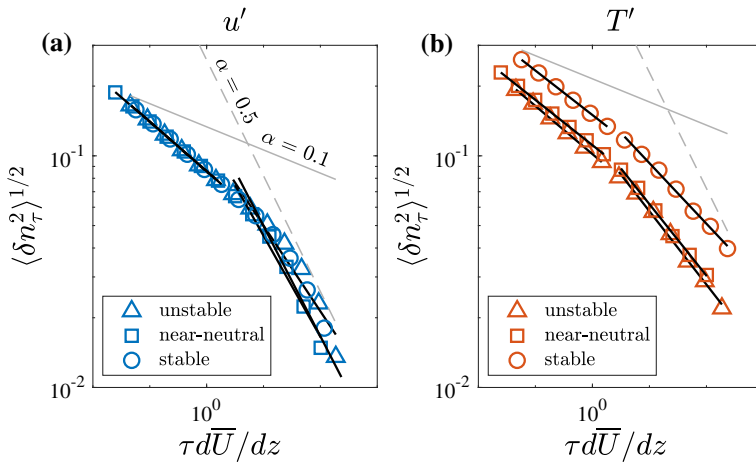


Fig. 7 As Fig. 6 but for the multi-point telegraphic approximation u' (a) and T' data (b)

In addition, this analysis was repeated in a multi-point framework by conditioning the TA series to be one at all heights, so that the occurrence of a coherent TA value ensures that all heights exceed their local mean simultaneously. That is, the multi-point telegraphic approximation is prescribed a value of one only when all available heights had positive turbulent excursions. This analysis serves as a generic telegraphic approximation that can assess the differences between u' and T' without regard to sampling height, and represents coherent clustering behaviour of large-scale motions across the range of heights sampled. The quantity $\langle \delta n_\tau^2 \rangle^{1/2}$ is plotted against $\tau d\bar{U}/dz$ for the multi-point telegraphic approximation in Fig. 7, where $(d\bar{U}/dz)^{-1}$ is calculated at $z = 1$ m and represents the mean shear time scale.

Lastly, to examine the effects of stability and distance from the surface on the clustering behaviour, profiles of α are presented in Fig. 8, with the results of the multi-point TA featured on the $z = 0$ axis. The following observations can be made:

1. The fine scales for both u' and T' exhibit higher clustering (lower α values) than the large scales. For the fine scales across both variables and under all three stability classes, $\alpha \in [0.23, 0.31]$, consistent with α values reported elsewhere for the fine scales (Sreenivasan and Bershadskii 2006).
2. Overall, distance from the ground does not seem to be a dynamically significant variable in clustering at all scales of both u' and T' . Despite a tenfold difference in measuring height, the clustering exponent was more or less vertically homogeneous under all stability conditions.
3. The fine scales of both u' and T' exhibit less scatter in α across the three stability classes in comparison to the large scales.
4. In the fine scales, the T' series exhibit slightly higher clustering than the corresponding u' series for the same stability conditions. The average α values across all sampling heights for u' and T' are 0.28 and 0.27, respectively, for near-neutral conditions, 0.30 and 0.27 for unstable conditions, and 0.29 and 0.25 for stable conditions.
5. The large scales of T' appear to be the most sensitive to atmospheric stability and exhibit higher clusterization (lower α values) under stable conditions. When compared to the corresponding u' signal, the T' series reveals higher clusterization u' under stable conditions, but lower clusterization under unstable conditions.

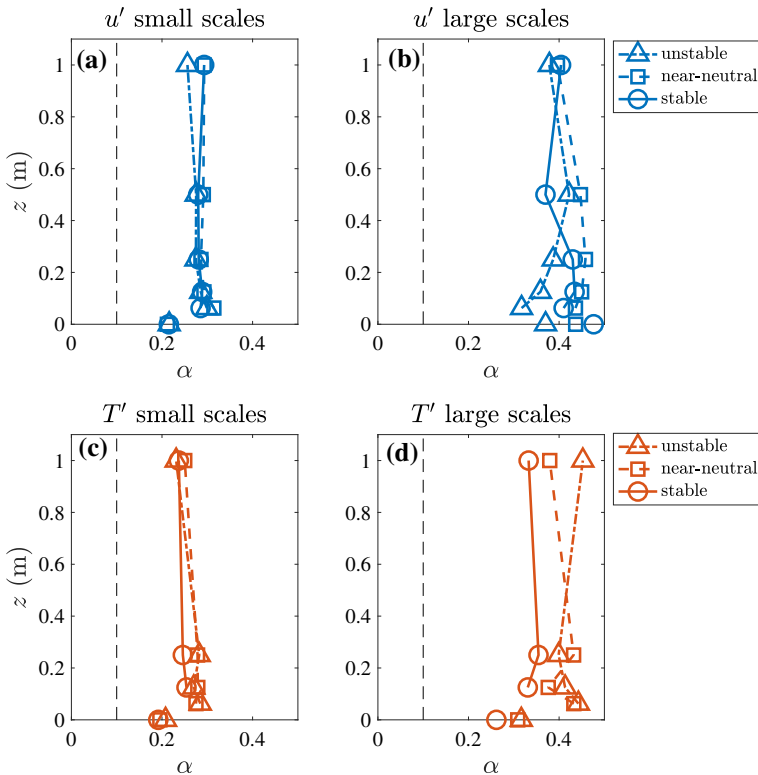


Fig. 8 Profiles of clustering exponents ensemble-averaged for each stability regime for the small scales of u' (a), the large scales of u' (b), the small scales of T' (c), and the large scales of T' (d). The data points on the $z = 0$ axis represent the clustering exponents of the multi-point telegraphic approximation for the corresponding variable and stability regime. The dashed vertical line indicates $\alpha = 0.1$ in the limit of infinite Re_λ

6. The coherent clustering behaviour of large-scale motions represented by the multi-point TA generally conforms to the observations above. The fine scales for both u' and T' exhibit similar clustering tendencies across all stability regimes with a value close to $\alpha = 0.2$. The large scales exhibit less clustering in comparison, with $\alpha > 0.33$. For the large scales, higher clustering in T' compared with u' was observed under all stability conditions.

As observed in other studies, the large scales exhibit less clustering and approach the white noise value of $\alpha = 0.5$, while the fine scales exhibit higher clustering (Sreenivasan and Bershadskii 2006; Cava and Katul 2009). The fine scales of both u' and T' appear less sensitive to atmospheric stability compared with the large scales, consistent with the idea that small-scale fluctuations approach local isotropy and are thus less affected by thermal instabilities. The large scales of T' , on the other hand, exhibit increased clustering with increasing atmospheric stability. This could be related to the non-stationary and localized shear produced by submesoscale motions, which are present in stable boundary layers (Anfossi et al. 2005). Increased clustering in T' compared with u' was also observed in the small scales for all stability conditions, the extent of which was most noticeable under stable conditions. This could be a signature of large-scale structures such as shear-driven ramps impacting scales in the inertial range, reflective of the connection between sharp fronts of ramp-cliff patterns and an excess time-derivative skewness magnitude in T' when compared to u' (Celani et al. 2001;

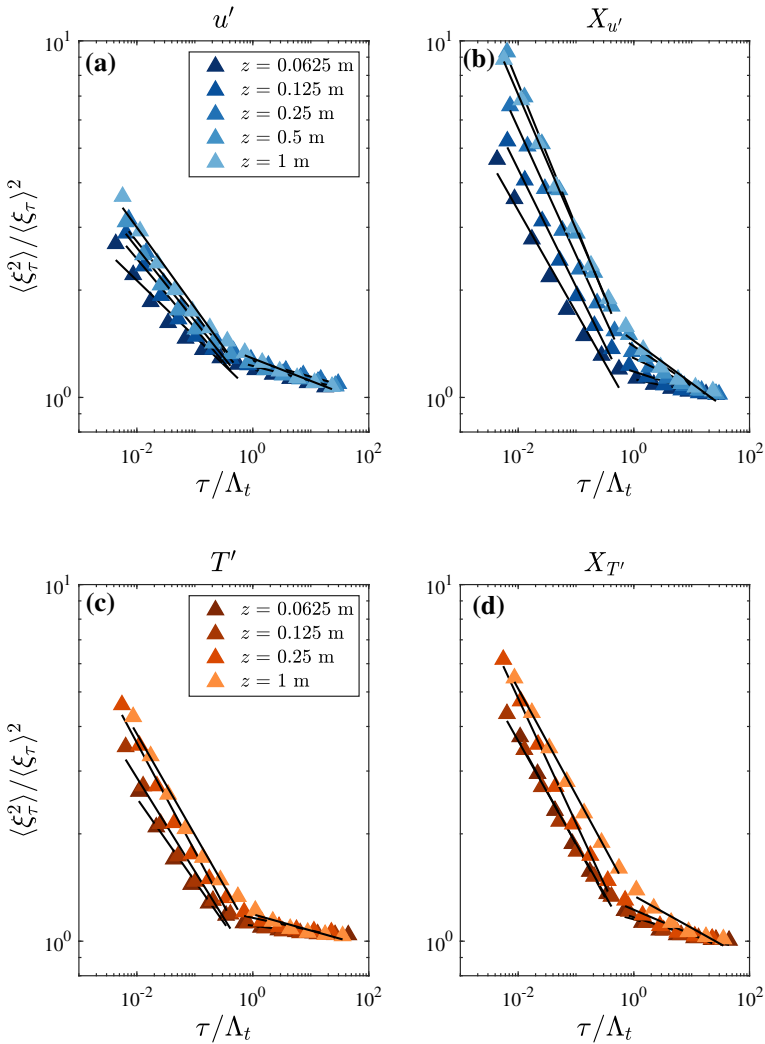


Fig. 9 Normalized second moment of the squared temporal gradients ensemble-averaged across datasets with unstable stability for u' and its corresponding TA series $X_{u'}$, (a) and (b) respectively, and for T' and its corresponding TA series $X_{T'}$, (c) and (d) respectively. The straight lines are best-fits that indicate the scaling laws for the two regions separated at $\tau / \Lambda_t \sim 1/6$

Katul et al. 2006; Zorzetto et al. 2018). Lastly, a multi-point TA analysis (a coherent TA value that takes on a value of one only when all heights exceed their local mean simultaneously) was performed and shown to conform largely with the observations above, thereby providing a generic TA framework that can assess differences between u' and T' without regard to distance from the ground.

4.4 Intermittency Exponents

The intermittency exponents μ_s and μ_{TA} were computed for both u' and T' for all three atmospheric stability conditions. As an example, the scaled second moment as described by

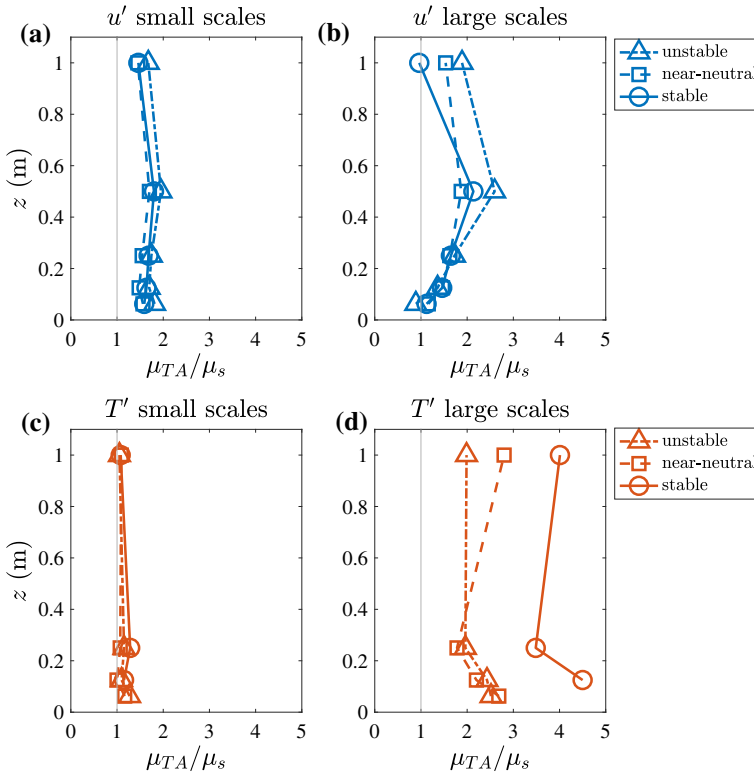


Fig. 10 Profiles of the ratio between μ_{TA} and μ_s ensemble-averaged across datasets with the same stability regime as given in Table 1, for the small scales of u' (a), the large scale of u' (b), the small scales of T' (c), and the large scales of T' (d)

Eq. 13 (with $q = 2$) against τ/Λ_t for the unstable condition is plotted in Fig. 9. Two distinctive scaling regimes are again present with separation at $\tau/\Lambda_t \sim 1$, permitting estimation of intermittency exponents in both fine and large scales. The demarcation was again taken to be $\tau/\Lambda_t = 1/6$ here. Profiles of the ratio μ_{TA}/μ_s are presented in Fig. 10. The following observations can be noted:

1. In both the small and large scales of u' , $\mu_{TA}/\mu_s > 1$ across all stability regimes, which suggests that amplitude variations weaken intermittency for u' .
2. By contrast, in the fine scales of T' , $\mu_{TA}/\mu_s \sim 1$ suggests that amplitude variations do not play a significant role in intermittency, so that much of the observed intermittency is due to clusterization.
3. The magnitude of μ_{TA}/μ_s is homogeneous across all stability conditions and all heights in the small scales of u' (where $\mu_{TA}/\mu_s \approx 1.5$) and of T' (where $\mu_{TA}/\mu_s \approx 1$).
4. The large scales of T' appear the most sensitive to stability conditions, with stable conditions yielding larger μ_{TA}/μ_s values than those under the unstable and near-neutral conditions, which are comparable. That is, stability seems to increase the role of amplitude variations in weakening the observed intermittency for the large scales of T' .

In the small scales of u' , amplitude variation seems to weaken intermittency, while in the small scales of T' , amplitude variations do not seem to play a role in the observed intermit-

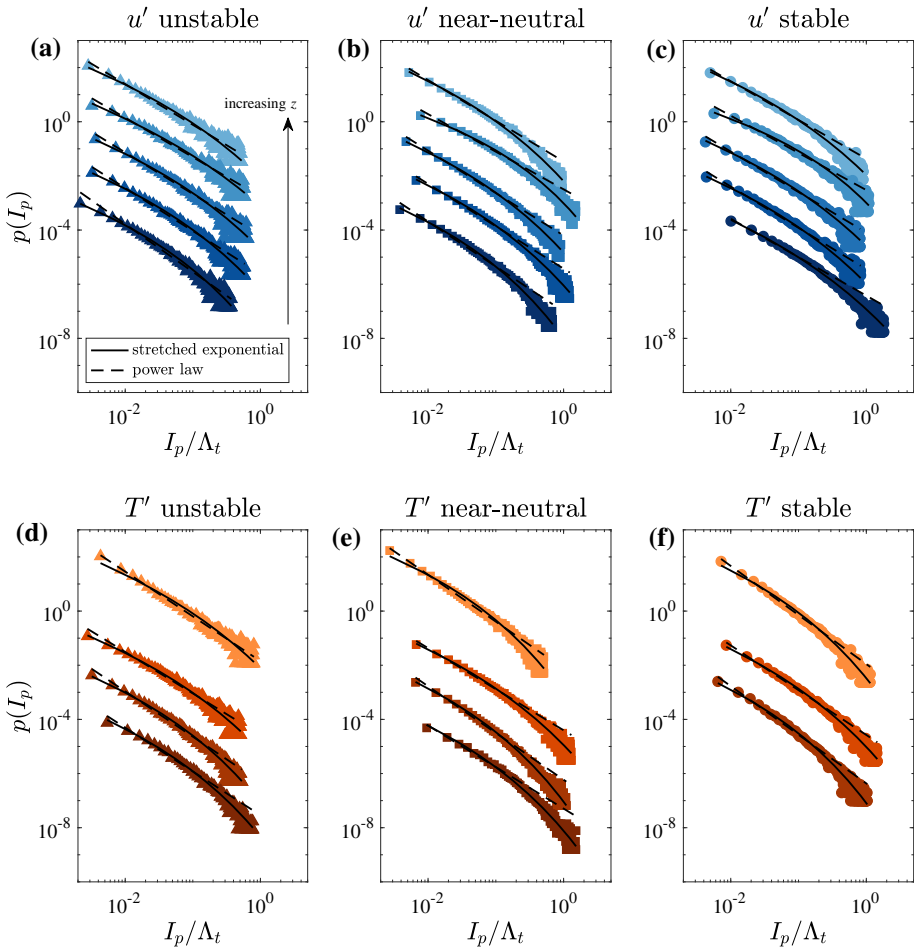


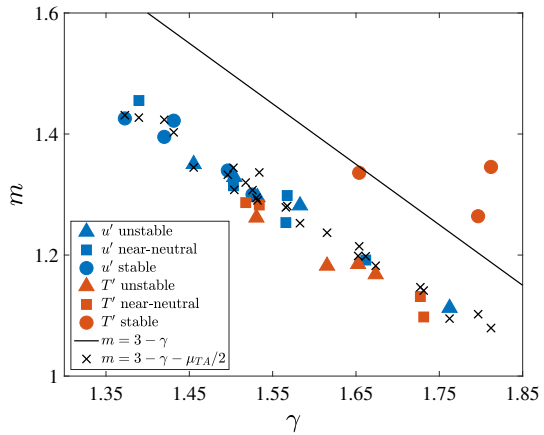
Fig. 11 Ensemble-averaged p.d.f.s of the inter-pulse period for each stability regime and for both u' and T' , offset to permit comparisons. The power-law fit is applied to $I_p/\Delta_t < 1/6$, and the legend for the sampling heights is the same as in Fig. 6

tency and much of the observed intermittency is due to clusterization. This observation is consistent with Cava and Katul (2009). The insensitivity of these μ_{TA}/μ_s ratios to thermal stability in the small scales is again reflective of the idea of smaller scales approaching local isotropy. By contrast, the large scales of T' appear the most sensitive to stability conditions, where the extent to which amplitude variation weakens intermittency increases with atmospheric stability. That is, as stability increases, the magnitude variations play an increasingly prominent role in smoothing the clusterization effects in the large scales of T' .

4.5 Probability Density Function of the Inter-pulse Period

The persistence p.d.f.s at all heights and under all stability regimes for both variables are presented in Fig. 11. The inter-pulse periods have been normalized by the respective integral time scales.

Fig. 12 Spectral exponent m (of the TA spectra) from the inertial subrange plotted against γ obtained from a power-law fit to the small inter-pulse periods ($I_p/\Lambda_t < 1/6$). For reference, $m = 3 - \gamma$ for systems near critical behaviour and its modification to account for intermittency are also plotted



The results presented here are consistent with the observations made by Chowdhuri et al. (2020), where the persistence p.d.f.s display a power-law behaviour at smaller I_p up to a threshold, then display an exponential cut-off. Here, it is evident that at small I_p , the power law is the optimal distribution for the persistence p.d.f. As I_p approaches Λ_t , the onset of an exponential cut-off can be seen. This picture can be shown statistically, with the stretched-exponential distribution providing a good fit to the persistence p.d.f.s ($R^2 > 0.93$) for all cases.

Overall, the persistence p.d.f. seems to follow different shapes in the various scaling regimes (much like the energy spectrum behaviour). The log-normal distribution shape as seen in Sreenivasan and Bershadskii (2006) for $I_p/\tau_d < 100$, where τ_d is a dissipative time scale, characterizes the smallest inter-pulse periods corresponding to the dissipative scales (which were beyond the sampling frequency of 100 Hz and thus not apparent in the current dataset). At longer inter-pulse periods commensurate with the inertial subrange, an approximate power law characterizes the persistence p.d.f., while at the longest inter-pulse periods corresponding to the energy-containing scales, an exponential tail describes the p.d.f. well.

To examine links between the small-scale turbulent behaviour and SOC processes, Fig. 12 presents the TA spectral exponent m from the inertial subrange against γ obtained from a power-law fit to small I_p (here, to $I_p/\Lambda_t = 1/6$). For all cases except the stable T' series, the dataset exhibits a linear behaviour that is close to that of the expected relation for systems near critical behaviour ($m = 3 - \gamma$), but with a lower intercept. Modification of the SOC relation to $m = 3 - \gamma - \mu_{TA}/2$ was able to significantly improve the agreement between measured and modelled m . However, some deviation still exists, mainly in the T' data, suggesting that there is excess intermittency not captured by μ_{TA} . This could be a signature of the presence of ramp-like patterns often found in scalars that tend to introduce extra intermittency and generate sharp edges, which have been shown to have an impact on inertial scales (Katul et al. 2006). By contrast, m and γ appear to be uncorrelated in T' under stable conditions, suggesting that the small-scale turbulent behaviour under stable conditions deviates from a SOC process. Overall, the SOC process seems a plausible model for small-scale-turbulence behaviour, at least within the confines of the TA framework.

5 Conclusions

The TA technique was applied to the streamwise velocity component u' and air temperature T' data taken in the first metre above the surface of salt flats. The current study utilizes nanoscale hot- and cold-wires with high spatial resolution, thereby permitting analysis with no spatial filtering effects, sampled at 100 Hz to capture inertial-range behaviour. The telegraphic approximation removes amplitude variations in turbulent excursions, and distills only clustering effects, one key component of intermittency. To examine dissimilarities in clustering behaviour of u' and T' , the spectral exponents and zero-crossing properties (including clustering, intermittency, and inter-pulse period distributions) were computed and relationships among them were analyzed across unstable, near-neutral, and stable regimes. This analysis extends studies that consider isolated clustering behavior without amplitude variations to the flow very near the surface (≤ 1 m) over a smooth terrain. In addition to the inertial subrange, which is the main focus of past studies, TA properties in the energy-containing region are presented and discussed.

Signatures of excess intermittency in T' as compared to u' can be seen in the clustering exponents, where it was shown that in the stable case, T' exhibits higher levels of clustering compared with u' in both the small and large scales. This suggests that the large-scale structures could also be impacting the inertial scales. When considering the relative ratio of intermittency exponents μ_{TA}/μ_s , most of the observed intermittency comes from clusterization in the small scales of T' (that amplitude variations play a comparatively negligible role in intermittency), and that the relative ratio of intermittency exponents in the large scales of T' is noticeably higher in magnitude compared with the respective u' counterparts (that is, the extent at which amplitude variability smooths out the signal is higher in T'). Generally, the distributional properties of the inter-pulse periods in u' and T' are similar, in which the persistence p.d.f. exhibits a power law at inter-pulse periods commensurate with the inertial scales, followed by an exponential cut-off at the larger inter-pulse periods, consistent with Chowdhuri et al. (2020). The TA properties share attributes with a SOC process by considering the relation between the power-law exponent of the persistence p.d.f. and the spectral exponent of the telegraphic approximation in the inertial subrange. Except for the stable T' data, the modified SOC relation $m = 3 - \gamma - \mu_{TA}/2$ is applicable for both flow variables and stabilities—at least under the confines of the TA framework—and displays signatures of excess intermittency in T' beyond the intermittency exponent μ_{TA} .

Due to the limited number of datasets in the current study and the positive skewness (as seen in Fig. 2), which is most often observed in the near-wall region (e.g. buffer region or roughness layer) where sweeps tend to dominate (see e.g. Heisel et al. 2020), whether the above findings are general and apply throughout the surface layer or are limited to near-surface phenomena remains to be explored. Nonetheless, the results here indicate that the TA approach is able to uncover dissimilarity between u' and T' across various thermal stratification levels and serve as a starting point for further studies concerning clustering within the ASL.

Acknowledgements This work was supported by the NSF-AGS-1649049. K. Huang was supported by the Department of Defense (DoD) through the National Defense Science and Engineering Graduate Fellowship (NDSEG) program, and G. Katul was supported by the NSF-AGS-1644382, NSF-AGS-2028644 and NSF-IOE-1754893. The authors also acknowledge Princeton University's Metropolis Project for partial support during Katul's sabbatical leave at Princeton University in 2020. The authors would also like to thank Matthew K. Fu for his help in editing this paper.

References

- Anfossi D, Öttl D, Degrazia G, Goulart L (2005) An analysis of sonic anemometer observations in low wind speed conditions. *Boundary-Layer Meteorol* 114(1):179–203
- Antonia R, Abe H, Kawamura H (2009) Analogy between velocity and scalar fields in a turbulent channel flow. *J Fluid Mech* 628:241
- Arwatz G, Fan Y, Bahri C, Hultmark M (2015) Development and characterization of a nano-scale temperature sensor (T-NSTAP) for turbulent temperature measurements. *Meas Sci Technol* 26(3):035103
- Bak P, Tang C, Wiesenfeld K (1988) Self-organized criticality. *Phys Rev A* 38(1):364
- Banerjee T, Katul G (2013) Logarithmic scaling in the longitudinal velocity variance explained by a spectral budget. *Phys Fluids* 25(12):125106
- Bendat JS, Piersol AG (2011) *Random data: analysis and measurement procedures*, vol 729. Wiley, New York
- Bershadskii A, Niemela J, Praskovsky A, Sreenivasan K (2004) “Clusterization” and intermittency of temperature fluctuations in turbulent convection. *Phys Rev E* 69(5):056314
- Cava D, Katul G (2009) The effects of thermal stratification on clustering properties of canopy turbulence. *Boundary-Layer Meteorol* 130(3):307
- Cava D, Katul GG, Molini A, Elefante C (2012) The role of surface characteristics on intermittency and zero-crossing properties of atmospheric turbulence. *J Geophys Res Atmos* 117(D1):D01104
- Cava D, Mortarini L, Giostra U, Acevedo O, Katul G (2019) Submeso motions and intermittent turbulence across a nocturnal low-level jet: A self-organized criticality analogy. *Boundary-Layer Meteorol* 172(1):17–43
- Celani A, Lanotte A, Mazzino A, Vergassola M (2001) Fronts in passive scalar turbulence. *Phys Fluids* 13(6):1768–1783
- Chambers A, Antonia R (1984) Atmospheric estimates of power-law exponents μ and μ_θ . *Boundary-Layer Meteorol* 28(3–4):343–352
- Chamecki M (2013) Persistence of velocity fluctuations in non-Gaussian turbulence within and above plant canopies. *Phys Fluids* 25(11):115110
- Chamecki M, Dias NL, Salesky ST, Pan Y (2017) Scaling laws for the longitudinal structure function in the atmospheric surface layer. *J Atmos Sci* 74(4):1127–1147
- Chowdhuri S, Kalmár-Nagy T, Banerjee T (2020) Persistence analysis of velocity and temperature fluctuations in convective surface layer turbulence. *Phys Fluids* 32(7):076601
- Citriniti J, George W (1997) The reduction of spatial aliasing by long hot-wire anemometer probes. *Exp Fluids* 23(3):217–224
- Fan Y, Arwatz G, Van Buren T, Hoffman D, Hultmark M (2015) Nanoscale sensing devices for turbulence measurements. *Exp Fluids* 56(7):138
- Gao W, Shaw R, et al (1989) Observation of organized structure in turbulent flow within and above a forest canopy. In: *Boundary layer studies and applications*. Springer, pp 349–377
- Garratt JR (1994) *The atmospheric boundary layer*. Cambridge University Press, Cambridge
- Giostra U, Cava D, Schipa S (2002) Structure functions in a wall-turbulent shear flow. *Boundary-Layer Meteorol* 103(3):337–359
- Heisel M, Katul GG, Chamecki M, Guala M (2020) Velocity asymmetry and turbulent transport closure in smooth-and rough-wall boundary layers. *Phys Rev Fluid* 5(10):104605
- Huang KY, Brunner CE, Fu MK, Kokmanian K, Morrison TJ, Perelet AO, Calaf M, Pardyjak E, Hultmark M (2021) Investigation of the atmospheric surface layer using a novel high-resolution sensor array. *Exp Fluids* 62(76):76
- Hutchins N, Chauhan K, Marusic I, Monty J, Klewicki J (2012) Towards reconciling the large-scale structure of turbulent boundary layers in the atmosphere and laboratory. *Boundary-Layer Meteorol* 145(2):273–306
- Jensen HJ, Christensen K, Fogedby HC (1989) $1/f$ noise, distribution of lifetimes, and a pile of sand. *Phys Rev B* 40(10):7425
- Kailasnath P, Sreenivasan K (1993) Zero crossings of velocity fluctuations in turbulent boundary layers. *Phys Fluids* 5(11):2879–2885
- Katul GG (1994) A model for sensible heat flux probability density function for near-neutral and slightly-stable atmospheric flows. *Boundary-Layer Meteorol* 71(1):1–20
- Katul G, Porporato A, Cava D, Siqueira M (2006) An analysis of intermittency, scaling, and surface renewal in atmospheric surface layer turbulence. *Physica D* 215(2):117–126
- Katul G, Konings A, Porporato A (2011) Mean velocity profile in a sheared and thermally stratified atmospheric boundary layer. *Phys Rev Lett* 107(26):268502
- Katul G, Porporato A, Nikora V (2012) Existence of k^{-1} power-law scaling in the equilibrium regions of wall-bounded turbulence explained by Heisenberg’s eddy viscosity. *Phys Rev E* 86(6):066311

- Klewicki J, Foss J, Wallace J (1998) High Reynolds number [$R_\theta = O(10^6)$] boundary layer turbulence in the atmospheric surface layer above western Utah's salt flats. In: Flow at ultra-high Reynolds and Rayleigh numbers. Springer, pp 450–466
- Li Q, Fu Z (2013) The effects of non-stationarity on the clustering properties of the boundary-layer vertical wind velocity. *Boundary-Layer Meteorol* 149(2):219–230
- Li D, Katul G, Gentine P (2016) The k^{-1} scaling of air temperature spectra in atmospheric surface layer flows. *Q J R Meteorol Soc* 142(694):496–505
- Liu L, Hu F (2020) Finescale clusterization intermittency of turbulence in the atmospheric boundary layer. *J Atmos Sci* 77(7):2375–2392
- Lumley J, Yaglom A (2001) A century of turbulence. *Flow Turbul Combust* 66(3):241–286
- Marusic I, Monty JP, Hultmark M, Smits AJ (2013) On the logarithmic region in wall turbulence. *J Fluid Mech* 716:R3
- Metzger M, Klewicki J (2001) A comparative study of near-wall turbulence in high and low Reynolds number boundary layers. *Phys Fluids* 13(3):692–701
- Morrison T, Calaf M, Higgins C, Drake S, Perelet A, Pardyjak E (2021) The impact of surface temperature heterogeneity on near-surface heat transport. *Boundary-Layer Meteorol*. <https://doi.org/10.1007/s10546-021-00624-2>
- Obukhov A (1962) Some specific features of atmospheric turbulence. *J Geophys Res* 67(8):3011–3014
- Perry AE, Henbest S, Chong MS (1986) A theoretical and experimental study of wall turbulence. *J Fluid Mech* 165:163–199
- Poggi D, Katul G (2009) Flume experiments on intermittency and zero-crossing properties of canopy turbulence. *Phys Fluids* 21(6):065103
- Pope SB (2000) *Turbulent flows*. Cambridge University Press, Cambridge
- Salesky S, Katul G, Chamecki M (2013) Buoyancy effects on the integral lengthscales and mean velocity profile in atmospheric surface layer flows. *Phys Fluids* 25(10):105101
- Shi B, Vidakovic B, Katul G, Albertson J (2005) Assessing the effects of atmospheric stability on the fine structure of surface layer turbulence using local and global multiscale approaches. *Phys Fluids* 17(5):055104
- Shraiman B, Siggia E (2000) Scalar turbulence. *Nature* 405(6787):639–646
- Sreenivasan K (1991) On local isotropy of passive scalars in turbulent shear flows. *Proc R Soc* 434(1890):165–182
- Sreenivasan KR, Antonia R (1997) The phenomenology of small-scale turbulence. *Annu Rev Fluid Mech* 29(1):435–472
- Sreenivasan K, Bershadskii A (2006) Clustering properties in turbulent signals. *J Stat Phys* 125(5–6):1141–1153
- Sreenivasan K, Prabhu A, Narasimha R (1983) Zero-crossings in turbulent signals. *J Fluid Mech* 137:251–272
- Sreenivasan K, Bershadskii A, Niemela J (2004) Multiscale SOC in turbulent convection. *Phys A Stat Mech Appl* 340(4):574–579
- Townsend A (1976) *The structure of turbulent shear flow*. Cambridge University Press, Cambridge
- Vallikivi M, Smits AJ (2014) Fabrication and characterization of a novel nanoscale thermal anemometry probe. *J Microelectromech Syst* 23(4):899–907
- Vallikivi M, Hultmark M, Smits AJ (2015) Turbulent boundary layer statistics at very high Reynolds number. *J Fluid Mech* 779:371
- Warhaft Z (2000) Passive scalars in turbulent flows. *Annu Rev Fluid Mech* 32(1):203–240
- Wei T, Fife P, Klewicki J, McMurtry P (2005) Properties of the mean momentum balance in turbulent boundary layer, pipe and channel flows. *J Fluid Mech* 522:303–327
- Wyngaard JC (2004) *Changing the face of small-scale meteorology*. In: Atmospheric turbulence and mesoscale meteorology. Cambridge University Press, Cambridge
- Zorzetto E, Bragg A, Katul G (2018) Extremes, intermittency, and time directionality of atmospheric turbulence at the crossover from production to inertial scales. *Phys Rev Fluids* 3(9):094604